Evidence for a Wind-Driven Intensification of the Kuroshio Current Extension from the 1970s to the 1980s

CLARA DESER

National Center for Atmospheric Research, Boulder, Colorado*

MICHAEL A. ALEXANDER AND MICHAEL S. TIMLIN

CIRES, Climate Diagnostics Center, University of Colorado, Boulder, Colorado

(Manuscript received 31 December 1997, in final form 2 July 1998)

ABSTRACT

The spatial and temporal characteristics of oceanic thermal variations in the mixed layer and main thermocline of the midlatitude North Pacific are distinctive, suggesting different physical origins. Within the main thermocline (400-m depth), the variability is dominated by a westward-intensified pattern of decadal scale, indicative of enhanced eastward geostrophic flow along the southern flank of the Kuroshio Current extension during the 1980s relative to the 1970s. The authors argue that the decadal-scale change in the strength of the Kuroshio extension was a result of the dynamical adjustment of the oceanic circulation to a decadal variation in wind stress curl according to Sverdrup theory. Four-times daily wind stress fields from the National Center for Atmospheric Research–National Centers for Environmental Prediction reanalysis project are used to compute the decadal change in Sverdrup transport associated with the 1976/77 climate transition. It is shown that the decadal changes in Sverdrup transport inferred from the wind stress curl field and in observed geostrophic flow inferred from the upper-ocean thermal field are consistent both in terms of spatial pattern and magnitude. The decadal change in depth-averaged geostrophic transport along the Kuroshio extension (referenced to 1 km) is 11.6 Sv, similar to the Sverdrup transport change (11.5–13.9 Sv). The decadal-scale thermocline variation along the western boundary between 30° and 40°N exhibits a lag of approximately 4–5 yr relative to the decadal variation in the basin-wide wind stress curl pattern. This delay may be indicative of the transient adjustment of the gyre-scale circulation to a change in wind stress curl via long baroclinic Rossby waves.

1. Introduction

There is increasing evidence for coherent decadal-scale fluctuations of the ocean–atmosphere system in the North Pacific (see Mantua et al. 1997 and Nakamura et al. 1997 for recent reviews). A particularly prominent example occurred from approximately 1977 to 1988, when sea surface temperatures (SSTs) were below normal across the central and western North Pacific and above normal along the west coast of North America. The SST anomalies were accompanied by a stronger than normal Aleutian low pressure system and associated midlatitude westerly winds, particularly during the winter half of the year (Fig. 1). Epipelagic marine ecosytems, including salmon production, were affected by the decadal climate change (Polovina et al. 1995; Brodeur et al. 1996; Mantua et al. 1997).

Several mechanisms have been proposed to explain the occurence of decadal-scale climate variations in the North Pacific. Decadal changes in tropical Pacific rainfall may force atmospheric teleconnections over the North Pacific (cf. Nitta and Yamada 1989; Trenberth 1990; Graham et al. 1994; Zhang et al. 1997), which in turn alter SSTs locally via turbulent energy fluxes, Ekman current advection, and vertical mixing (Alexander 1992; Luksch and von Storch 1992; Miller et al. 1994). Local extratropical air–sea interaction may amplify the tropically induced decadal signal over the North Pacific, as suggested by Trenberth (1990), Trenberth and Hurrell (1994), and Yukimoto et al. (1996). Alternatively, the dynamical adjustment of the extratropical ocean circulation via long baroclinic Rossby waves to stochastic wind stress forcing may lead to SST variability on decadal timescales, independent of the Tropics (Frankignoul et al. 1997; Jin 1997). Latif and Barnett (1994; see also Robertson 1996 and Jin 1997) argue that coupled extratropical air–sea interaction involving ocean gyre

* The National Center for Atmospheric Research is sponsored by the National Science Foundation.

Corresponding author address: Dr. Clara Deser, Climate and Global Dynamics Division, NCAR, P.O. Box 3000, Boulder, CO 80307-3000.
E-mail: cdeser@ucar.edu

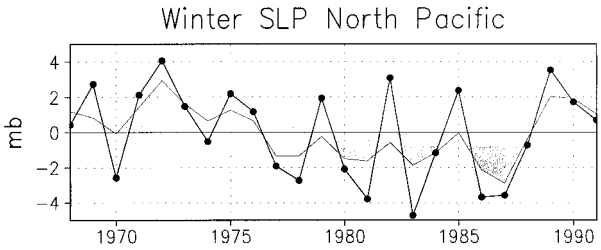

FIG. 1. Time series of winter (Nov–Mar) SLP (mb) averaged over the central North Pacific (30°–65°N, 160°E–140°W). The solid circles denote the raw winter SLP anomalies, and the shaded curve the anomalies smoothed with a three-point binomial filter. This record is a reliable indicator of the leading mode of wintertime atmospheric circulation variability over the North Pacific. After Trenberth and Hurrell (1994).

dynamics may result in self-sustained decadal-scale oscillations of the North Pacific climate system.

Clearly, it is important to extend the observational description of decadal-scale variability in the North Pacific from the sea surface to the ocean interior. Does the large-scale oceanic circulation exhibit decadal fluctuations, and if so, to what extent are the changes wind driven? Recent analyses of upper-ocean thermal structure have begun to address these questions. Deser et al. (1996) and Miller et al. (1998) documented a westward-intensified pattern of decadal-scale thermal anomalies in the main pycnocline (400-m depth) in midlatitudes. Using thermal wind arguments, they inferred that the eastward geostrophic flow of the Kuroshio Current extension was enhanced during the 1980s relative to the 1970s (see also Yasuda and Hanawa 1997). A similar decadal-scale increase in eastward transport of the Kuroshio Current south of Japan was reported by Qiu and Joyce (1992). The decadal transport variations of the Kuroshio Current system were interpreted by Miller et al. (1998) as a response to large-scale wind forcing based on experiments with an ocean general circulation model, a result also anticipated by Trenberth (1990), Qiu and Joyce (1992), and Yasuda and Hanawa (1997). Wind forcing was also implicated in the observed decadal-scale change of the Alaska gyre circulation reported by Lagerloef (1995).

A more passive role for the oceanic circulation was indicated by Watanabe and Mizuno (1994), Deser et al. (1996), Lysne et al. (1997), and Schneider et al. (1999), who showed that thermal anomalies originating in the deep winter mixed layer in the central North Pacific can become subducted into the upper portion of the main thermocline and subsequently transported downward and equatorward along isopycnal surfaces by the mean subtropical gyre circulation. A warm anomaly during the 1970s and a cold anomaly during the 1980s were advected by the mean circulation from the central North Pacific to approximately 18°N in the western Pacific over a period of approximately 8 yr, following closely the model of the ventilated thermocline (Schneider et al. 1999). Elements of the ''ventilated thermocline'' signal can also be found in Zhang and Levitus (1997), who showed that at 250-m depth thermal anomalies appear to rotate clockwise around the subtropical gyre over the course of approximately a decade.

The simplest theory of the steady-state response of the large-scale oceanic circulation to wind stress forcing is the Sverdrup relation (Sverdrup 1947). Simply stated, the Sverdrup relation is a linear vorticity balance between wind stress curl and meridional advection of planetary vorticity by interior flows; zonal currents are inferred from mass continuity considerations. Thus, the large-scale distribution of wind stress curl determines the gyre-scale patterns of the oceanic circulation. Note that Sverdrup balance does not account for the strong western boundary currents that complete the gyre circulations.

There is considerable debate over the extent to which Sverdrup balance governs the observed large-scale oceanic circulation, particularly in the Atlantic sector, given the neglect of important processes such as interaction of the flow with bottom topography, thermohaline effects, and inertial and recirculation components (cf. Wunsch and Roemmich 1985). However, despite its simplicity, Sverdrup balance appears to account quantitatively for much of the large-scale circulation in the North Pacific (cf. Niiler and Koblinsky 1985; Qiu and Joyce 1992; Hautala et al. 1994; Kagimoto and Yamagata 1997).

Miller et al. (1998) invoked Sverdrup theory to explain the decadal strengthening of the Kuroshio Current system in an ocean general circulation model forced with observed wind stress and heat flux anomalies from 1970 to 1988. The purpose of this study is to provide additional observational support for the hypothesis that the decadal-scale increase in the transport of the Kuroshio extension was a result of large-scale wind stress forcing according to simple Sverdrup dynamics. In particular, we shall demonstrate that the decadal-scale changes in observed geostrophic flow inferred from the upper-ocean thermal field and Sverdrup transport inferred from the wind stress curl field are similar in both their spatial pattern and magnitude.

2. Data and methods

a. Ocean temperature dataset

The subsurface ocean temperature profiles used in this study are from the *World Ocean Atlas 1994* (*WOA94*; Levitus and Boyer 1994). These data were recovered as part of a recent and extensive search through international archives and then quality controlled in a consistent manner (Boyer and Levitus 1994). Here we examine thermal variations in the upper 450 m of the North Pacific (20°–55°N) from 1968 to 1991 using data from three sources (mechanical bathythermographs, expendable bathythermographs, and station data consisting primarily of Nansen bottles); however, expendable bathy-

thermographs (XBTs) account for the majority of the observations during this time period (see Levitus and Boyer 1994; Deser et al. 1996). Our choice of study period was dictated by the density of subsurface temperature profiles available from the *WOA94*, and the lower limit for our analysis (450 m) reflects the deepest level routinely sampled by the XBTs.

Characteristics of the spatial and temporal distributions of the data may be found in Levitus and Boyer (1994) and Deser et al. (1996). Here we note simply that the subsurface archive contains an order of magnitude fewer observations than surface marine datasets such as the Comprehensive Ocean–Atmosphere Data Set (COADS; Woodruff et al. 1987). However, as discussed in Deser et al. (1996), the relatively sparse sampling of the subsurface network appears adequate nevertheless for the study of decadal-scale variations in the north Pacific.

As in Deser et al. (1996), we formed monthly anomalies on a 1° × 1° grid at each standard level from the surface to 400 m as departures from the Levitus and Boyer (1994) objectively analyzed monthly 1° × 1° climatology. The 1° × 1° anomalies were then averaged into 2° lat × 4° long grid boxes. We have made no attempt to fill in missing data. Further information concerning data distribution, gridding procedures, and validation techniques may be found in Timlin et al. (1995) and Deser et al. (1996).

We shall also make use of thermal profiles extending to 1-km depth in the far western Pacific, obtained from Nansen bottle casts.

b. Wind stress dataset

The surface wind stress data are from the National Center for Atmospheric Research–National Centers for Environmental Prediction (NCEP–NCAR) reanalysis project (Kalnay et al. 1996) for the period 1968–91 (1968 was the earliest year available at the time this study was undertaken). The reanalysis project uses a fixed state-of-the art global data assimilation system and a comprehensive observational database to derive dynamically consistent atmospheric fields. As such, it represents one of the most complete and quality controlled archives of atmospheric data currently available.

Wind stress is computed four times daily on a T62 Gaussian grid (roughly equivalent to 2° lat × 2° long) using a bulk aerodynamic formula in which the drag coefficient depends on both wind speed and static stability according to Businger et al. (1971). For further information regarding the boundary layer scheme in the assimilation model, the reader is referred to Kanamitsu (1989).

Other studies rely on purely observational archives such as the COADS to derive surface wind stresses over the ocean. However, spurious trends in COADS wind speeds due to changes in observing practices (cf. Cardone et al. 1990; Cayan 1992; Ward and Hoskins 1996), coupled with the relatively sparse spatial and temporal sampling of the ship-of-opportunity network, led us to adopt the reanalysis wind stress product for our study.

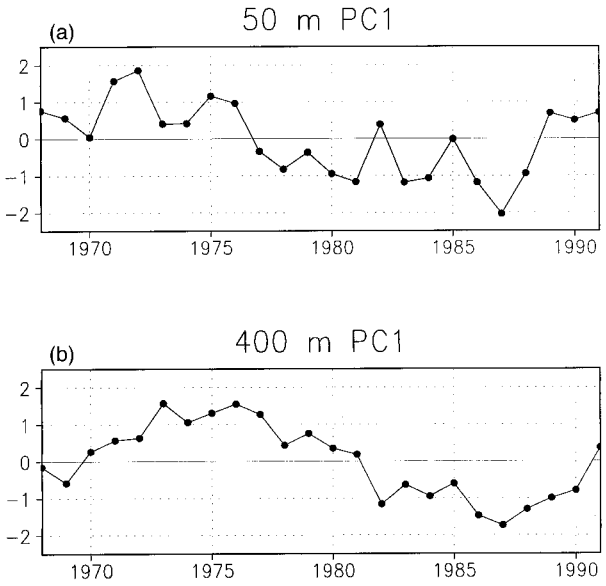

FIG. 2. Leading principal component of annual subsurface temperature anomalies in the North Pacific. Units are standard deviations. (a) 50 m. (b) 400 m.

c. EOF analysis

To define the dominant structures of variability in the subsurface thermal field, we apply empirical orthogonal function (EOF) analysis to the covariance matrix of annual anomalies on a 4° × 4° grid based on the period 1968–91. Annual anomalies are defined as January–December averages of the individual monthly departures from the monthly long-term means. The domain for the EOF analyses is 24°–56°N, 150°E–120°W. The principal component time series are obtained by projecting the spatial EOF patterns onto the original anomaly fields for each year.

3. Results

a. Upper-ocean thermal variability

Figure 2 shows the leading principal component time series of annual temperature anomalies at 50- and 400-m depth, which account for 37% and 26% of the variance, respectively. The 50-m record represents thermal variations within the winter mixed layer (summer mixed layer depths are less than 20–30 m), while the 400-m record is indicative of conditions in the permanent thermocline below the winter mixed layer. The leading principal component at 50 m (Fig. 2a) is similar to the winter sea level pressure (SLP) time series shown in Fig. 1: the correlation between them is 0.82 (0.90 after smoothing with a three-point binomial filter). Note, however,

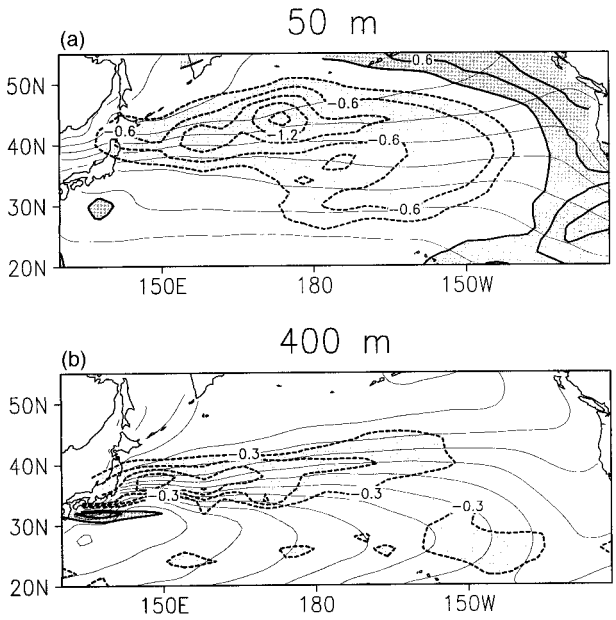

FIG. 3. (a) Decadal-scale change in annual temperature at 50 m (thick contours; negative values are dashed), formed by subtracting the period 1968–76 from the period 1977–88. The contour interval is 0.3°C, and the zero contour has been omitted. The thin contours denote the long-term mean temperature field. (b) As above but for 400 m, formed by subtracting the period 1970–80 from the period 1982–90.

that the decadal signal is more prominent in the oceanic thermal field than in SLP (relative to interannual variations). Decadal-scale changes are even more pronounced (relative to interannual changes) at 400 m (Fig. 2b) than at 50 m. The decadal variation at 400 m is delayed relative to that at 50 m, with the transition from positive to negative anomalies occuring in 1981/82 rather than 1976/77.

On the basis of the principal component time series, we identified a warm period (1968–76 at 50 m and 1970–80 at 400 m) and a cold period (1977–88 at 50 m and 1982–90 at 400 m). Figure 3 shows the spatial patterns of the difference between the cold and warm periods (these maps resemble closely the EOF patterns upon which they are based). The decadal-scale change at 50 m (Fig. 3a) exhibits a basin-wide pattern, with negative anomalies in excess of -0.6°C in the central and western Pacific, and positive anomalies of similar magnitude along the west coast of North America. This pattern closely resembles the decadal change of SST in winter (not shown, but see comparable figures in Trenberth and Hurrell 1994; Deser et al. 1996; Zhang et al. 1997; Nakamura et al. 1997, among others). In contrast, the decadal-scale change at 400 m (Fig. 3b) exhibits a westward-intensified pattern with the largest cooling (in excess of -0.6°C) centered along approximately 35°N and weaker warming directly south of Japan. The strongest cooling lies along the axis of maximum meridional temperature gradient that marks the path of the Kuroshio Current extension. The regional warming south of Japan may reflect a weaker Kuroshio meander after 1982 as shown in Qiu and Joyce (1992). A similar westward-intensified pattern of 400-m thermal variability was shown by Miller et al. (1998) based upon extended EOF analysis, a technique that accomodates propagating as well as stationary signals. The negative anomaly centered near 25°N and 150°W may be associated with subduction as documented by Deser et al. (1996) and Schneider et al. (1999). Note the absence of positive temperature anomalies in the eastern third of the basin at 400 m.

The distinctive spatial and temporal signatures of the decadal-scale temperature changes in the mixed layer and the main thermocline suggests that they are controlled by different physical processes. Ocean modeling studies have shown that the basin-scale pattern of thermal variability within the winter mixed layer is largely a result of anomalous fluxes of latent and sensible energy at the sea surface due to changes in atmospheric circulation (cf. Alexander 1992; Luksch and von Storch 1992; Miller et al. 1994), although wind-induced anomalous advection by Ekman currents and entrainment may also contribute in certain locations. The large simultaneous correlation between the 50-m temperature principal component and the winter Aleutian low SLP index is consistent with the rapid (order 1 month) thermal response of the winter mixed layer to anomalous turbulent energy fluxes (Frankignoul 1985; Deser and Timlin 1997). The main thermocline, on the other hand, isolated from direct thermodynamic contact with the atmosphere, adjusts to changes in atmospheric circulation via dynamical processes. We proceed next to test the hypothesis that the decadal-scale change of temperature at 400 m resulted from the dynamical adjustment of the oceanic circulation to changes in wind stress curl according to Sverdrup's (1947) theory.

b. Sverdrup balance

Sverdrup balance may be derived from the vertical integral of the linear vorticity equation,

$$\beta v = f\frac{\partial w}{\partial z},$$

where v is the meridional velocity, f is the Coriolis parameter, β is the latitudinal gradient of the Coriolis parameter, and w is the vertical velocity. Integrating this equation from a depth, z_o, where the vertical velocity is assumed to vanish, to the base of the surface Ekman layer where the vertical velocity is assumed to result from wind-driven convergence or divergence in the surface Ekman layer, one obtains the familiar form of Sverdrup balance:

$$\beta V_g = \frac{f}{\rho_o}\mathbf{k}\cdot\nabla\times\left(\frac{\tau}{f}\right), \quad (1)$$

where V_g is the vertically integrated meridional geostrophic transport, ρ_o (=1025 kg m^{-3}) is the density of seawater, $\mathbf{k}$ is the unit vector in the vertical direction, $\tau = (\tau^\lambda, \tau^\phi)$ is the wind stress vector, and ∇ is the gradient operator in spherical coordinates. Equation (1) states that the input of relative vorticity to the ocean by the wind stress curl will result in water parcels moving northward in order to conserve their total (relative + planetary) vorticity. Note that the right-hand side of Eq. (1) is the Sverdrup transport $[(1/\rho_o)\mathbf{k} \cdot \nabla \times \tau]$ minus the Ekman transport $[-(\beta/\rho_o f) \cdot \tau^\lambda]$. For the decadal-scale changes considered here, the Ekman term is less than 3% of the Sverdrup term.

If one defines a two-dimensional streamfunction (ψ_g) for the depth-integrated geostrophic velocity,

$$V_g = -\frac{\partial \psi_g}{\partial x}, \qquad U_g = \frac{\partial \psi_g}{\partial y},$$

then Eq. (1) can be rewritten as

$$\psi_g(x) = -\frac{f}{\beta \rho_o} \int_{x_E}^{x} \mathbf{k} \cdot \left(\nabla \times \frac{\tau}{f} \right) dx', \qquad (2)$$

where x_E represents the eastern boundary of the ocean basin where we have assumed $\psi_g(x_E) = 0$. Thus according to Sverdrup theory, the geostrophic transport is related to the zonal integral of the wind stress curl from the eastern boundary. Note that Eq. (2) is evaluated at each latitude separately.

c. Wind stress curl forcing

Next we derive the decadal change in ψ_g from the observed wind stress curl field and compare it to the decadal change in the observed geostrophic flow inferred from the depth-averaged thermal field. Since annual mean wind stresses drive the large-scale oceanic circulation on decadal timescales, we first examine the leading mode of variability of annual wind stress anomalies. The leading principal component (not shown), which accounts for 48% of the variance, is very similar to the record of winter SLP in the Aleutian low (Fig. 1): the correlation between them is 0.92 (0.95 after smoothing with a three-point binomial filter).

Figure 4 shows the decadal-scale change in annual wind stress and its curl, formed by subtracting the period 1968–76 from the period 1977–88. The mean annual wind stress and curl fields are also shown for reference. Decadal westerly wind stress anomalies cover much of the basin, with maximum values (approximately 0.02 N m^{-2} or 30%–60% of the mean) between 30° and 40°N, at the southern flank of the mean westerly wind stress belt (see Fig. 4, top). The strongest decadal westerly wind stress anomalies are straddled by a north–south curl dipole between approximately 25° and 40°N. This anomalous curl dipole extends across nearly two-thirds of the basin, from 150°E to 140°W, with maximum values of $2 - 4 \times 10^{-8}$ N m^{-3}. Because of its zonal elongation, the curl dipole has important consequences for the Sverdrup transport (see below). Note that the anomalous curl dipole is located south of the climatological zero wind stress curl line (see Fig. 4a) that delineates the northern boundary of the mean oceanic subtropical gyre.

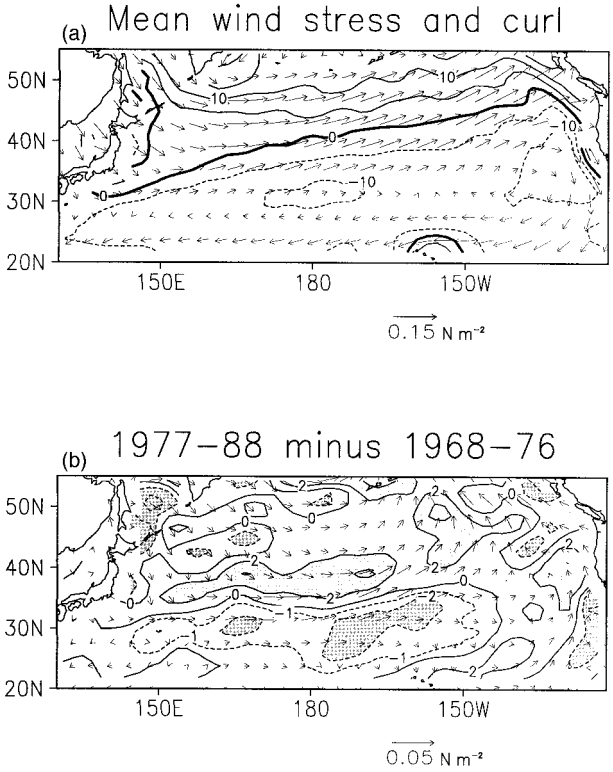

FIG. 4. (a) Long-term mean annual wind stress (vectors; N m^{-2}) and its curl (contours; 10^{-8} N m^{-3}) from the NCEP–NCAR reanalyses for the period 1968–91. The contour interval is 5×10^{-8} N m^{-3}, the zero curl line is darkened, and negative values are dashed. The scale for the vectors is indicated at the lower right. (b) Decadal-scale change in annual wind stress (vectors) and its curl (contours), formed by subtracting the period 1968–76 from the period 1977–88, based on the NCEP–NCAR reanalyses. The contour interval is 2×10^{-8} N m^{-3} and values greater than 2×10^{-8} N m^{-3} (less than -2×10^{-8} N m^{-3}) are indicated with light (dark) shading. The -1×10^{-8} N m^{-3} contour is also shown for clarity. Note that the wind vector scale and contour interval differ from those shown in (a).

Integrating the curl field westward from the coast of North America according to (2) yields the geostrophic (Sverdrup minus Ekman) transport streamfunction (Fig. 5). Note that the direction of the transport is parallel to contours of the streamfunction field, with the strength inversely proportional to the contour spacing. The climatological mean Sverdrup (minus Ekman) transport shows the familiar pattern of anticyclonic flow around the subtropical gyre and cyclonic flow around the subpolar gyre (Fig. 5a). The maximum strength of the subtropical (subpolar) gyre along the western boundary is 43 Sv (1 Sv = 10^9 kg s^{-1}) at 30°N (44 Sv at 56°N). Similar mean Sverdrup transport fields were shown by

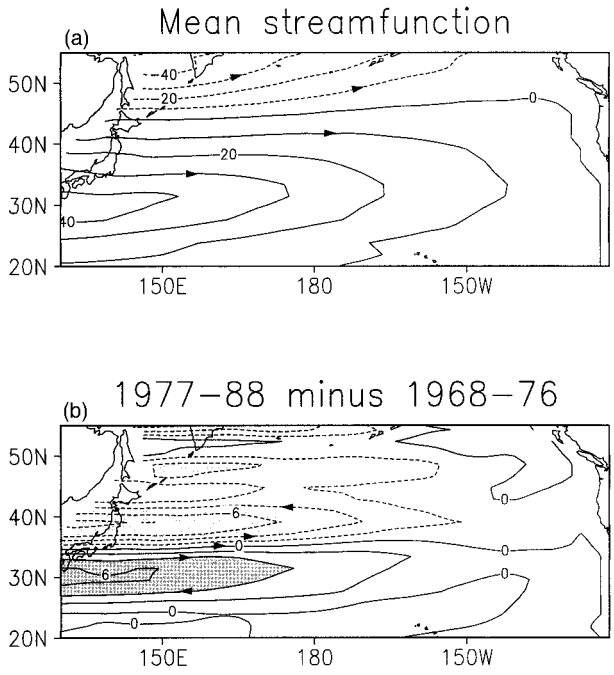

FIG. 5. (a) Long-term mean annual geostrophic (Sverdrup minus Ekman) transport streamfunction. The contour interval is 10 Sv, with negative values dashed. (b) Decadal-scale change in annual geostrophic (Sverdrup minus Ekman) transport streamfunction, formed by subtracting the period 1968–76 from the period 1977–88. The contour interval is 2 Sv, with negative values dashed. Values greater than 4 Sv (less than −4 Sv) are indicated with dark (light) shading.

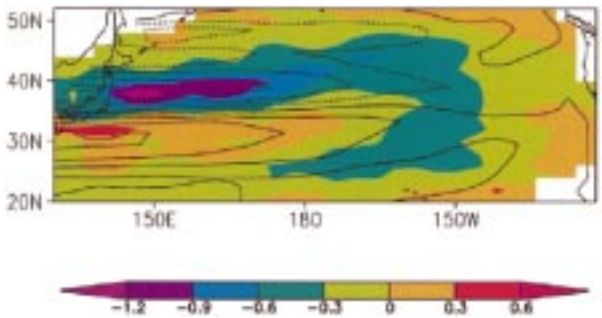

FIG. 6. Decadal-scale change in annual geostrophic (Sverdrup minus Ekman) transport streamfunction (thick black contours, taken from Fig. 5) superimposed upon the decadal-scale change in vertically integrated temperature from 0 to 450 m (color shading). The decadal-scale thermal anomalies were formed by subtracting the period 1970–80 from the period 1982–90.

Trenberth et al. (1990) and Yasuda and Hanawa (1997), although our values for the subtropical gyre are slightly lower than those in Trenberth et al.

Like the mean Sverdrup transport distribution, the decadal difference is westward intensified, with maximum positive anomalies of 6 Sv at 30°N and maximum negative anomalies of −8 Sv at 38°N along the western boundary (Fig. 5b). Enhanced eastward transport is indicated between 30° and 38°N, along the southern flank of the region of climatological mean eastward flow (Fig. 5a). The decadal strengthening of the subtropical gyre, as measured by the maximum streamfunction value at 30°N, is approximately 15%. Similar decadal-scale differences in Sverdrup transport were shown by Trenberth (1991), Yasuda and Hanawa (1997), and Miller et al. (1998).

d. Comparison of Sverdrup and observed geostrophic flow

How well do the geostrophic (Sverdrup minus Ekman) transport streamfunction (ψ_g) differences match the observed upper-ocean thermal changes? Note that a low in ψ_g should correspond to an upward displacement of the thermocline (low heat content) resulting from positive wind stress curl, and a high to a depressed thermocline (high heat content) resulting from negative wind stress curl. Figure 6 shows the decadal-scale change in ψ_g superimposed upon the decadal change in vertically integrated temperature from 0 to 450 m. Note that the thermal difference is lagged relative to the streamfunction change in accord with the results shown in Figs. 1–3. The two fields are in good spatial agreement west of 170°W, with below-normal heat content corresponding to below-normal streamfunction centered along 38°N, and above-normal heat content corresponding to above-normal streamfunction centered along 30°N east of 150°E. (The peak thermal anomaly west of 145°E is displaced slightly north of the corresponding high in ψ_g.) Both fields indicate enhanced eastward flow between 30° and 38°N, using thermal wind arguments to infer geostrophic flow from the thermal field. The negative ψ_g anomaly center near 47°N, 150°E has no counterpart in the thermal field. Conversely, the negative thermal anomalies extending from 25°N, 180° northeastward to 34°N, 150°W do not correspond with the ψ_g field and, as mentioned above, may result from anomalous subduction.

The spatial structures of the decadal anomalies in heat content and ψ_g are compared further in Fig. 7, which shows latitudinal profiles of the two fields averaged across the western Pacific (142°–175°E). The meridional structure of the two fields is similar, with negative values between approximately 36° and 42°N, and positive values between approximately 28° and 32°N. However, in addition to a small constant offset between the two quantities, the positive streamfunction anomalies between approximately 25° and 33°N are enhanced relative to the thermal anomalies. As shown below, the reduced amplitude of the heat content anomalies relative to the streamfunction changes south of 33°N reflects that the thermal anomalies extend well below 450 m in this region.

To estimate quantitatively the geostrophic tranport from the heat content observations, the vertical structure of the thermal changes down to a ''level of no motion'' is required. The studies of Qiu and Joyce (1992) and

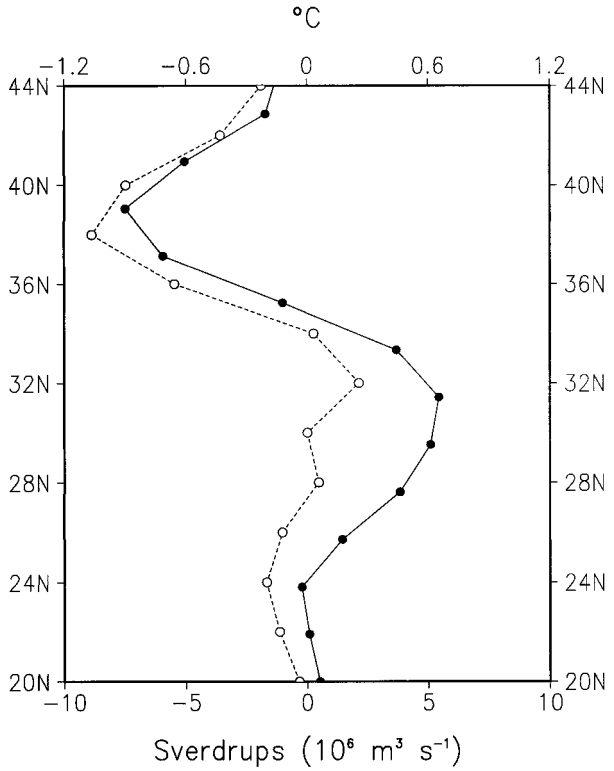

FIG. 7. Latitudinal structure of the decadal-scale change in geostrophic (Sverdrup minus Ekman) transport streamfunction (solid curve) and vertically integrated temperature from 0 to 450 m (dashed curve) averaged across the western half of the Pacific (142°–176°E).

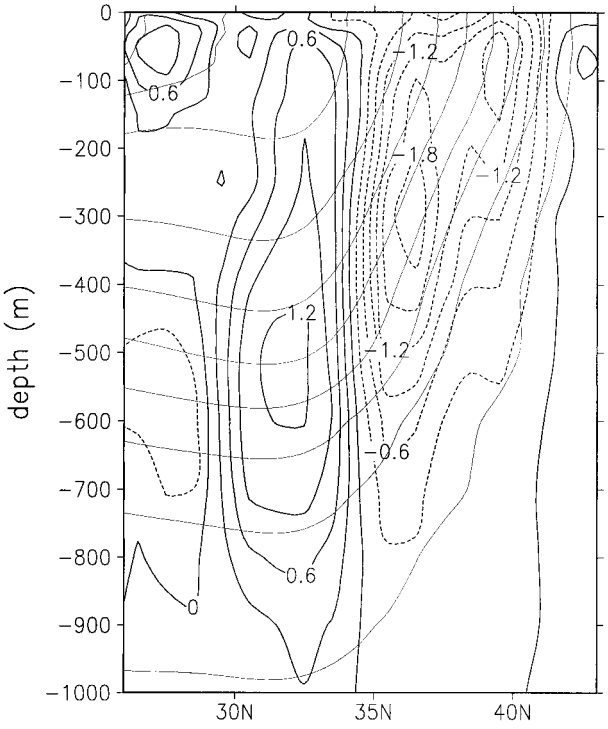

FIG. 8. Latitude–depth cross section of the decadal-scale temperature change in the far western Pacific (142°–150°E; thick contours) superimposed upon the long-term mean thermal field (thin contours). The contour interval for the decadal differences is 0.3°C, with negative values dashed. The contour interval for the mean field is 2°C.

Huang and Russell (1994) suggest that this level is approximately 1–1.5 km for the subtropical gyre. To extend the decadal-scale thermal changes down to 1 km, we used the station data (Nansen bottle) archives (on a 1° × 1° grid) from the *WOA94*. The sparsity of Nansen bottle observations precludes basin-wide maps of the decadal changes below 500 m. Fortunately, the data density is highest in the far western Pacific (25°–43°N, 142°–150°E), where the decadal-scale thermal variations are largest. However, the results should be considered preliminary until more observations below 500 m are obtained.

Figure 8 shows the vertical structure of the decadal-scale thermal changes in the upper kilometer for the far western Pacific as a function of latitude, superimposed upon the climatological mean temperature distribution. The thermal anomalies exhibit little tilt with depth and reach a maximum in the main thermocline. Thus, the largest positive anomaly (1.2°C), located at 32°N, is centered around 500–600-m depth, well below the maximum level sampled by the XBTs, whereas the the largest negative anomaly (−1.8°C), located at 37°N, is situated considerably shallower, near 300-m depth.

Using the profiles shown in Fig. 8 and climatological salinity profiles from Levitus and Boyer (1994), we computed the decadal change in the depth-averaged geostrophic current (referenced to 1 km) between 32° and 37°N (the extrema in the vertically integrated thermal anomaly field). The resulting decadal change in the geostrophic transport is 11.6 Sv. For comparison, the decadal change in geostrophic transport inferred from the wind stress curl field is 11.5 Sv between 32° and 37°N (13.9 Sv between 31.5° and 39°N, the extrema in the Sverdrup transport field). We note that different wind stress products may yield different estimates for the Sverdrup-minus-Ekman transport; however, decadal *changes* in the transport should be relatively insensitive to the wind stress formulation, barring any systematic trends.

Our estimate of the decadal change in geostrophic zonal transport east of Japan may be compared with flow variations upstream in the Kuroshio south of Japan given in Qiu and Joyce (1992). Qiu and Joyce used biannual hydrographic surveys along 137°E conducted by the Japanese Meteorological Agency from 1967 to 1988 to compute the geostrophic transport of the Kuroshio, defined as the total eastward flow north of 30°N referenced to a depth of 1.25 km. Their Kuroshio transport record, shown in Fig. 9, displays a gradual increase from the mid-1970s to the early 1980s. The decadal change from 1970–80 to 1982–88 is 10.8 Sv, similar to our estimate for the Kuroshio Extension.

It is instructive to view the decadal changes not only

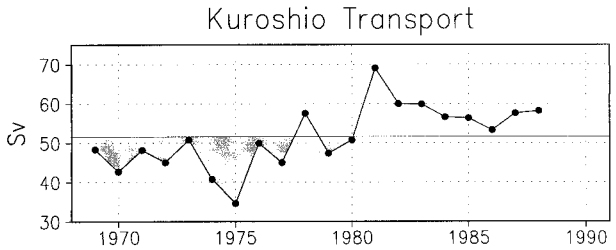

FIG. 9. Time series of geostrophic eastward transport Sverdrups (Sv) of the Kuroshio Current south of Japan referenced to 1.25 km, taken from Qiu and Joyce (1992). The thin horizontal line denotes the mean transport during 1969–88 (51.7 Sv).

in terms of anomalies from the climatological mean, but also in terms of the total flow. Figure 10a shows the latitudinal structure of the total geostrophic zonal flow averaged between the surface and 1 km in the far western Pacific (142°–150°E) for the periods 1970–80 and 1982–90. Analogous profiles for the total zonal wind stress averaged across the Pacific (150°E–140°W) for the periods 1968–76 and 1977–88 are shown in Fig. 10b. The midlatitude eastward flows in both the ocean and atmosphere intensified along their southern flanks from the 1970s to the 1980s, with the largest increases (38% of the mean) at 35°N in both fields.

4. Discussion

In agreement with Miller et al. (1998), our results suggest that the recent decadal-scale change in annual wind stress curl over the North Pacific altered the strength of the Kuroshio Current extension in a manner consistent with Sverdrup dynamics. Compared to the 1970s, the 1980s were characterized by an equatorward intensification of the mean midlatitude eastward flows in both the atmosphere and ocean.

The dynamical adjustment of the midlatitude oceanic gyre circulation to a decadal-scale change in wind stress curl is accomplished largely by westward-propagating first-mode baroclinic Rossby waves (cf. Anderson and Gill 1975). At low frequencies and long wavelengths, these Rossby waves are zonally nondispersive. If the duration of the anomalous wind stress curl forcing is greater than the time it takes the forced Rossby wave to cross the basin, then the gyre circulation will be in quasi-equilibrium with the winds, a state described by Sverdrup balance. For the case examined here, the winds are predominantly stronger than normal for about 11 yr (1977–88; recall Fig. 1) and predominantly weaker than normal for at least 15 yr (1962–76; not shown, but see the expanded record shown in Trenberth and Hurrell 1994). The Rossby wave transit time is approximately 3.5–6 yr assuming a group velocity of 3–5 cm s^{-1} appropriate for the latitude band 30°–40°N (based on recent satellite altimetry measurements; see Chelton and Schlax 1996) and a zonal extent for the wind forcing of 60° longitude from the western boundary (recall Fig. 4). Thus, the duration of the wind stress curl forcing is at least twice the transit time of the long baroclinic Rossby wave, indicating that Sverdrup balance may be expected to be achieved over the decadal time averages considered here. We note that the Rossby wave speeds derived from recent satellite altimetry measurements (cf. Chelton and Schlax 1996) are nearly twice as fast as

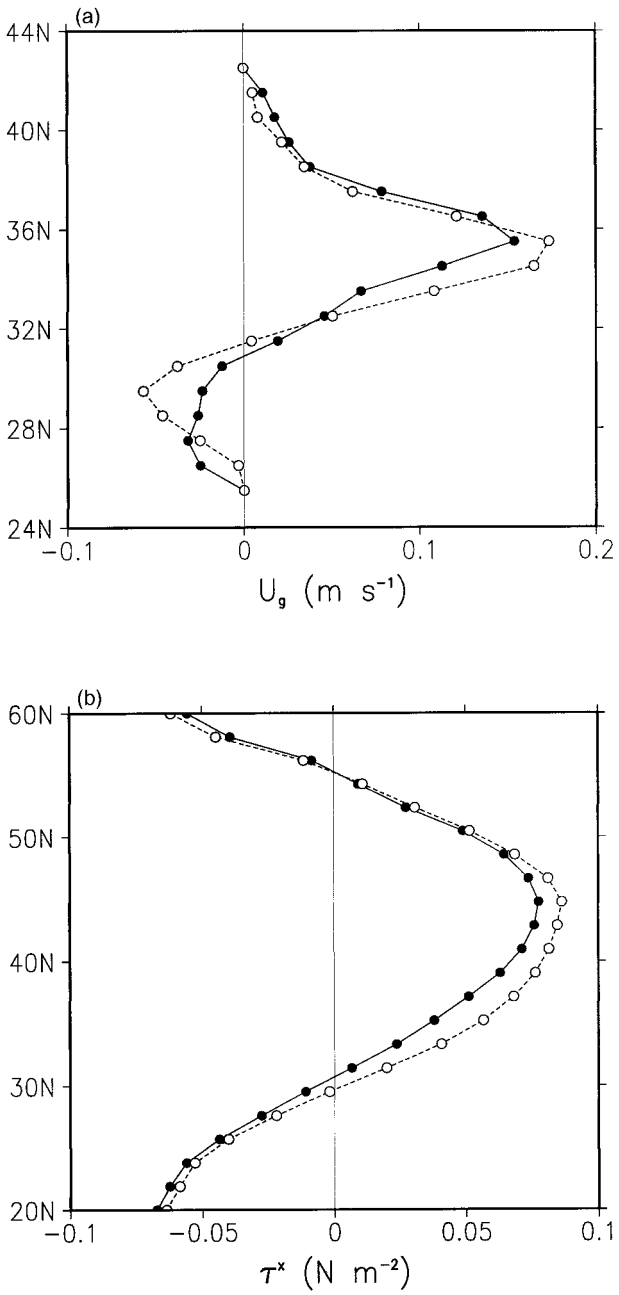

FIG. 10. (a) Latitudinal structure of the total geostrophic zonal flow averaged between the surface and 1 km (m s^{-1}) in the far western Pacific (142°–150°E) for 1970–80 (solid curve) and 1982–90 (dashed curve). (b) As in (a) but for the total zonal wind stress (N m^{-2}) averaged across the Pacific (150°E–140°W) for 1968–76 (solid curve) and 1977–88 (dashed curve).

predicted by linear theory, but can be reconciled with more modern theoretical treatments (Killworth et al. 1997; Qiu et al. 1997).

The results indicate a 4–5-yr delay between the decadal-scale variation in thermocline depth near the western boundary and the basin-wide wind stress curl pattern (recall Figs. 1 and 2). The observed delay is roughly consistent with that expected from the Rossby wave adjustment process as discussed above. It is also worth noting that the observed vertical structure of the decadal-scale thermal change (specifically the amplitude maximum within the main thermocline seen in Fig. 8) is consistent with the signature of a first-mode baroclinic Rossby wave that has its maximum vertical velocity in the main thermocline. However, ocean modeling experiments are needed to substantiate whether the observed delay and vertical structure are dynamically consistent with the Rossby wave adjustment process.

Other thermal signals extending down into the main pycnocline have been reported in association with the mid-1970s climate transition. For example, Watanabe and Mizuno (1994), Deser et al. (1996), and Schneider et al. (1999) identified an apparent subducted thermal anomaly in the main thermocline of the central North Pacific during the 1980s and traced its movement southwestward and downward following the mean subtropical gyre circulation, in accord with the theory of the ventilated thermocline. We view the diabatically induced subduction anomaly as distinct from the thermal signal associated with the dynamical spinup of the gyre circulation documented here, due to differences in both location and timing.

Zhang and Levitus (1997) present some evidence for decadal-scale anticyclonic rotation of subsurface thermal anomalies around the subtropical gyre. This advective signal is most apparent at 250-m depth, with little systematic movement indicated at the sea surface or at 400 m (Zhang and Levitus). The lack of movement at 400-m depth is consistent with the findings of Miller et al. (1998) and our own analyses (not shown), which indicate that the westward-intensified pattern of thermal anomalies at 400 m (e.g., Fig. 3) is, to first order, a stationary feature that grows and decays in place on the decadal timescale. The clockwise movement at 250 m may be associated with anomalous subduction as described above, particularly since this depth lies within the ventilated thermocline zone. Further work is needed to understand the different spatial and temporal characteristics of decadal-scale thermal variations at 250- and 400-m depth.

It is interesting to speculate about the possible future effects of the southward-intensified subtropical gyre circulation during the 1980s. According to the paradigm put forth by Latif and Barnett (1994), increased poleward heat transport by a stronger subtropical gyre may lead to a reduction of the meridional sea surface temperature gradient, which in turn may diminish the strength of the zonal wind stress, resulting in a weakening of the gyre over the next decade or two. Further observational and modeling experiments are needed to evaluate the realism of this scenario.

5. Conclusions

The purpose of this study was to test the hypothesis that the westward-intensified pattern of decadal-scale temperature change at 400-m depth in the North Pacific resulted from the dynamical adjustment of the oceanic circulation to changes in wind stress curl according to Sverdrup theory. Using 6-hourly wind stress curl data from the NCEP–NCAR reanalyses and upper-ocean thermal profiles from the *WOA94*, we demonstrated that the spatial patterns of the decadal-scale change in Sverdrup transport streamfunction and heat content in the upper 450 m are very similar. We extended the thermal data down to 1-km depth to estimate quantitatively the decadal-scale changes in geostrophic transport along the Kuroshio extension and found good agreement with the wind stress curl induced changes in transport (11.6 vs 11.5–13.9 Sverdrups). It remains to be seen whether the observed 4–5-yr delay of the thermocline anomalies in the western portion of the subtropical gyre relative to the decadal-scale wind stress curl forcing is physically consistent with the Rossby wave adjustment process.

Acknowledgments. We wish to thank Drs. Arthur Miller, Ping Chang, William Large, and Peter Gent for helpful discussions during the course of this work. The graphics were produced with the GrADS software package developed at the University of Maryland.

REFERENCES

Alexander, M., 1992: Midlatitude atmosphere–ocean interaction during El Niño. Part I: The North Pacific Ocean. *J. Climate,* **5,** 944–958.

Anderson, D. L. T., and A. E. Gill, 1975: Spin-up of a stratified ocean, with application to upwelling. *Deep-Sea Res.,* **22,** 583–596.

Boyer, T., and S. Levitus, 1994: Quality control and processing of histroical oceanographic temperature, salinity and oxygen data. NOAA Tech. Rep. NESDIS 81, 64 pp. [Available from National Oceanic and Atmospheric Administration, U.S. Govt. Printing Office, Washington, DC 20402.]

Brodeur, R. D., B. W. Frost, S. R. Hare, R. C. Francis, and W. J. Ingraham Jr., 1996: Interannual variations in zooplankton biomass in the Gulf of Alaska and covariation with California Current zooplankton biomass. *Calif. Coop. Oceanic Fish. Invest. Rep.,* **37,** 80–99.

Businger, J., A. C. Wyngaard, Y. Izumi, and E. F. Bradley, 1971: Flux-profile relationships in the atmospheric surface layer. *J. Atmos. Sci.,* **28,** 181–189.

Cardone, V. J., J. G. Greenwood, and M. A. Cane, 1990: On trends in historical marine data. *J. Climate,* **3,** 113–127.

Cayan, D., 1992: Variability of latent and sensible heat fluxes over estimated using bulk formulae. *Atmos.–Ocean,* **30,** 1–42.

Chelton, D. B., and M. G. Schlax, 1996: Global observations of oceanic Rossby waves. *Science,* **272,** 234–238.

Deser, C., and M. S. Timlin, 1997: Atmosphere–ocean interaction on weekly timescales in the North Atlantic and Pacific. *J. Climate,* **10,** 393–408.

——, M. A. Alexander, and M. S. Timlin, 1996: Upper ocean thermal

variations in the North Pacific during 1970–1991. *J. Climate,* **9,** 1840–1855.

Frankignoul, C., 1985: Sea surface temperature anomalies, planetary waves and air–sea feedback in the middle latitudes. *Rev. Geophys.,* **23,** 357–390.

——, C. Duchene, and E. Zorita, 1997: A simple model of the decadal response of the ocean to stochastic wind forcing. *J. Phys. Oceanogr.,* **27,** 1533–1546.

Graham, N. E., T. P. Barnett, R. Wilde, M. Ponater, and S. Schubert, 1994: On the roles of tropical and midlatitude SSTs in forcing interannual to interdecadal variability in the winter Northern Hemisphere circulation. *J. Climate,* **7,** 1416–1442.

Hautala, S. L., D. H. Roemmich, and W. J. Schmitz, 1994: Is the North Pacific in Sverdrup balance along 24° N? *J. Geophys. Res.,* **99,** 16 041–16 052.

Huang, R. X., and S. Russell, 1994: Ventilation of the subtropical North Pacific. *J. Phys. Oceanogr.,* **24,** 2589–2604.

Jin, F.-F., 1997: A theory of interdecadal climate variability of the North Pacific ocean–atmosphere system. *J. Climate,* **10,** 1821–1835.

Kagimoto, T., and T. Yamagata, 1997: Seasonal transport variations of the Kuroshio: An OGCM simulation. *J. Phys. Oceanogr.,* **27,** 403–418.

Kalnay, E., and Coauthors, 1996: The NCEP/NCAR 40-Year Reanalysis Project. *Bull. Amer. Meteor. Soc.,* **77,** 437–471.

Kanamitsu, M., 1989: Description of the NMC global data assimilation and forecast system. *Wea. Forecasting,* **4,** 335–342.

Killworth, P. D., D. B. Chelton, and R. A. de Szoeke, 1997: The speed of observed and theoretical long extratropical planetary waves. *J. Phys. Oceanogr.,* **27,** 1946–1966.

Lagerloef, G. S. E., 1995: Interdecadal variations in the Alaska Gyre. *J. Phys. Oceanogr.,* **25,** 2242–2258.

Latif, M., and T. P. Barnett, 1994: Causes of decadal climate variability over the North Pacific and North America. *Science,* **266,** 634–637.

Levitus, S., and T. P. Boyer, 1994: *World Ocean Atlas 1994. NOAA Atlas NESDIS,* Vol. 4, *Temperature,* NOAA/NESDIS, 117 pp.

Luksch, U., and H. von Storch, 1992: Modeling the low frequency sea surface temperature variability in the North Pacific. *J. Climate,* **5,** 893–906.

Lysne, J., P. Chang, and B. Giese, 1997: Impact of the extratropical Pacific on equatorial variability. *Geophys. Res. Lett.,* **24,** 2589–2592.

Mantua, J. N., S. R. Hare, Y. Zhang, J. M. Wallace, and R. C. Francis, 1997: A Pacific interdecadal climate oscillation with impacts on salmon production. *Bull. Amer. Meteor. Soc.,* **78,** 1069–1080.

Miller, A. J., D. R. Cayan, T. P. Barnett, N. E. Graham, and J. M. Oberhuber, 1994: Interdecadal variability of the Pacific Ocean: Model response to observed heat flux and wind stress anomalies. *Climate Dyn.,* **9,** 287–302.

——, ——, and W. B. White, 1998: A westward-intensified decadal change in the North Pacific thermocline and gyre-scale circulation. *J. Climate,* **11,** 3112–3127.

Nakamura, H., G. Lin, and T. Yamagata, 1997: Decadal climate variability in the North Pacific during recent decades. *Bull. Amer. Meteor. Soc.,* **78,** 2215–2225.

Niiler, P. P., and C. J. Koblinsky, 1985: A local time-dependent Sverdrup balance in the eastern North Pacific Ocean. *Science,* **229,** 754–756.

Nitta, T., and S. Yamada, 1989: Recent warming of tropical sea surface temperature and its relationship to the northern hemisphere circulation. *J. Meteor. Soc. Japan,* **67,** 375–383.

Polovina, J. J., G. T. Mitchum, and G. T. Evans, 1995: Decadal and basin-scale variation in mixed layer depth and the impact on biological production in the central and North Pacific, 1960–1988. *Deep-Sea Res.,* **42,** 1701–1716.

Qiu, B., and T. M. Joyce, 1992: Interannual variability in the mid- and low- latitude western North Pacific. *J. Phys. Oceanogr.,* **22,** 1062–1079.

——, W Miao, and P. Muller, 1997: Propagation and decay of forced and free baroclinic Rossby waves in off-equatorial oceans. *J. Phys. Oceanogr.,* **27,** 2405–2417.

Robertson, A. W., 1996: Interdecadal variability over the North Pacific in a multi-century climate simulation. *Climate Dyn.,* **12,** 227–241.

Schneider, N., A. J. Miller, M. A. Alexander, and C. Deser, 1999: Subduction of decadal North Pacific temperature anomalies: Observations and dynamics. *J. Phys. Oceanogr.,* **29,** 1056–1070.

Sverdrup, H., 1947: Wind-driven currents in a baroclinic ocean; with application to the equatorial currents of the eastern Pacific. *Proc. Natl. Acad. Sci.,* **33,** 318–326.

Timlin, M. S., M. A. Alexander, and C. Deser, 1995: Upper Ocean thermal changes in the North Pacific during 1970–1992. *19th Annual Climate Diagnostic Workshop,* College Park, MD, NOAA/NWS and Climate Prediction Center, 338–341.

Trenberth, K. E., 1990: Recent observed interdecadal climate changes in the Northern Hemisphere. *Bull. Amer. Meteor. Soc.,* **71,** 988–930.

——, 1991: Recent climate changes in the Northern Hemisphere. DOE Workshop. *Greenhouse-Gas-Induced Climate Change: A Critical Appraisal of Simulations and Observations,* M. Schlesinger, Ed., Elsevier, 377–390.

——, and J. W. Hurrell, 1994: Decadal atmosphere–ocean variations in the Pacific. *Climate Dyn.,* **9,** 303–319.

——, W. G. Large, and J. G. Olson, 1990: The mean annual cycle in global ocean wind stress. *J. Phys. Oceanogr.,* **20,** 1742–1760.

Ward, M. N., and B. J. Hoskins, 1996: Near-surface wind over the global ocean. *J. Climate,* **9,** 1877–1895.

Watanabe, T., and K. Mizuno, 1994: Decadal changes of the thermal structure in the North Pacific. *Int WOCE News lett.,* **15,** 10–13.

Woodruff, S. D., R. J. Slutz, R. L. Jenne, and P. M. Steurer, 1987: A comprehensive ocean–atmosphere data set. *Bull. Amer. Meteor. Soc.,* **68,** 1239–1250.

Wunsch, C., and D. Roemmich, 1985: Is the North Atlantic in Sverdrup balance? *J. Phys. Oceanogr.,* **15,** 1876–1880.

Yasuda, T., and K. Hanawa, 1997: Decadal changes in the mode waters in the midlatitude North Pacific. *J. Phys. Oceanogr.,* **27,** 858–870.

Yukimoto, S., M. Endoh, Y. Kitamura, A. Kitoh, T. Motoi, A. Noda, and T. Tokioka, 1996: Interannual and interdecadal variabilities in the Pacific in an MRI coupled GCM. *Climate Dyn.,* **12,** 667–683.

Zhang, R. H., and S. Levitus, 1997: Structure and cycle of decadal variability of upper-ocean temperature in the North Pacific. *J. Climate,* **10,** 710–727.

Zhang, Y., J. M. Wallace, and D. S. Battisti, 1997: ENSO-like interdecadal variability: 1900–1993. *J. Climate,* **10,** 1004–1020.